

Phantom matter: a challenging solution to the cosmological tensions

Adrià Gómez-Valent, Joan Solà Peracaula

Departament de Física Quàntica i Astrofísica,
and Institute of Cosmos Sciences,
Universitat de Barcelona, Av. Diagonal 647, E-08028 Barcelona, Catalonia, Spain

E-mails: agomezvalent@icc.ub.edu, sola@fqa.ub.edu

Abstract. The idea of composite dark energy (DE) is quite natural since on general grounds we expect that the vacuum energy (associated to the cosmological term Λ) may appear in combination with other effective forms of DE, denoted X . This was indeed the old proposal from 2006 (cf. Ref. [42]), called the ‘ Λ XCDM model’. In the current work, we deal with a simplified version of this model and exploit the possibility that X behaves as ‘phantom matter’ (PM), which appears in stringy versions of the running vacuum model (RVM). Unlike phantom DE, it satisfies the strong energy condition like usual matter, hence bringing to bear positive pressure at the expense of negative energy. Bubbles of PM may appear in the manner of a transitory ‘phantom vacuum’ tunneled into the late universe before it heads towards a new de Sitter era, thereby offering a crop field for the growing of structures earlier than expected. Using SNIa, cosmic chronometers, transversal BAO, LSS data and the full CMB likelihood from Planck 2018, we find that the tensions virtually disappear in this stringy RVM scenario characterized by axionic dark matter. The value of H_0 emerging from our analysis proves compatible with SH0ES to within less than 0.25σ and the LSS growth tension is nonexistent. The statistical information criteria point to very strong evidence in favor of the PM solution. Finally, our approach favors quintessence-like behavior of the DE below $z \simeq 1.5$ at $\gtrsim 3\sigma$ CL, which is compatible with the recent DESI measurements.

1 Introduction

The standard (or concordance) cosmological model, aka Λ CDM, has been a rather successful paradigm for the description of the universe for more than three decades [1], especially since the late nineties [2]. Despite it constitutes the main theoretical pillar at our hands for the description of the universe’s evolution within the General Relativity (GR) context, the Λ CDM is being pestered by a number of glitches and hitches which prove to be more and more difficult to iron out. While the model is presumably right in the main (at least at a pure phenomenological level), an increasing number of worrisome inconsistencies (or “tensions”) have been perturbing its reputation and its future prospects. For a long time the role played by a rigid cosmological constant (CC) Λ in the standard Λ CDM model has been rather successful since it has provided a fairly reasonable description of the overall cosmological data [3, 4]. But the use of the cosmological term has never been fully clarified at the formal theoretical level since it is usually associated to the so-called “cosmological constant problem”, a serious conundrum which has been amply discussed in the literature, see e.g. [5–9] and references therein. Inasmuch as the vacuum energy density (VED) is related to Λ through $\rho_{\text{vac}} = \Lambda/(8\pi G_N)$ (G_N being Newton’s gravitational coupling), the conceptual fate of Λ is tied to our ultimate understanding of the VED on fundamental physical terms. Fortunately, recent theoretical developments on the VED in quantum field theory (QFT) are bringing new light for a potential alleviation of these theoretical difficulties. In fact, the possibility that the quantum vacuum (and hence that Λ itself) is actually dynamical (i.e. evolving with the cosmological expansion) rather than being stuck at a rigid value, has lately been substantiated in the context of quantum field theory in curved spacetime as well as in the framework of low-energy effective string theory [8–11]. For a long time, the dynamics of the VED has been popularly addressed on phenomenological grounds using ad hoc scalar fields (quintessence and the like) which supplant the role of the Λ -term through the current value of some suitable effective potential [6, 7], see e.g. [12] for a recent review. Currently, the first data release of the Dark Energy Spectroscopic Instrument (DESI) suggests tantalizing evidence that the dark energy (DE) might be dynamical using some common parameterizations of the DE [13]. More detailed analyses will be needed before getting a final confirmation, of course, but it is a fact that some anticipatory (and fairly robust) hints of dynamical DE in the literature already pointed out this possibility a few years ago from different perspectives and using a significant amount of cosmological data. The level of evidence was substantial and ranged in between $3 - 4\sigma$. Some of these analysis are well-known [14–18] and involved the running vacuum model (RVM)¹. Subsequent analysis around the same time supported also this possibility using different methods and parameterizations [20, 21].

Dynamical DE could also impinge positively on the resolution of the cosmological tensions. Let us recall that these are mainly concerned with the measurement of the current Hubble parameter $H_0 \equiv 100h$ km/s/Mpc and the growth of large scale structures (LSS). The latter is usually monitored with S_8 or σ_8 , or even better using a parameter σ_{12} defining the amplitude of the matter power spectrum at fixed spheres of radius 12 Mpc rather than $8h^{-1}$ Mpc, thus avoiding artificial dependence on the value of h [22–24]². The first kind of tension involves a serious disagreement between the CMB observations, using fiducial Λ CDM cosmology, and the local direct (distance ladder) measurements of the Hubble parameter today. It is arguably the most puzzling open question and it leads to a severe inconsistency of $\sim 5\sigma$ CL. between the mentioned observables. The second kind of tension is related with the exceeding rate of large scale structure formation in the late universe predicted by the Λ CDM as compared to measurements, although the discordance here is moderate, at a confidence level of $\sim 2 - 3\sigma$. More recently, data from the James Webb Space Telescope (JWST) [29, 30] have revealed the existence of an unexpectedly large population

¹For a review, see e.g. [8, 9, 19] and references therein

²See [25, 26] for summarized explanations about each of these tensions, and [27, 28] for comprehensive reviews.

of extremely massive galaxies at large redshifts $z \gtrsim 5 - 10$, a fact which is also strongly at odds with the prospects of the concordance model.

There is a wide panoply of strategies in the literature trying to mitigate some of the above tensions, although at present we may be still far away from a satisfactory resolution of the situation. We mention only a few. It has been argued that within the class of models where the DE is dealt with as a cosmic fluid with equation of state (EoS) $w(z)$, solving the H_0 tension demands the phantom condition $w(z) < -1$ at some z , whereas solving both the H_0 and σ_8 tensions requires $w(z)$ to cross the phantom divide and/or other sorts of exotic transitions, see e.g. [31–37]. The possibility of a sign flip of the Λ term has been entertained in recent times, e.g. in [38]. Let us also mention the model analyzed in [39, 40] (based on the framework of [41]), in which one considers a sudden transition from anti-de Sitter (AdS), hence $\Lambda < 0$, into de Sitter (dS) regime ($\Lambda > 0$) occurring near our time. Despite it being essentially ad hoc, the model yields a rather good fit to the data when transversal BAO is employed in the fitting analysis, see also [37]. Actually, a more general framework already existed since long ago, namely the Λ XCDM model [42–44], where the running vacuum and an extra X component can exchange energy. In this context, one can have $\Lambda < 0$ or $\Lambda > 0$.

In this work, we further exploit the virtues of the Λ XCDM class, which is an enhanced version of the RVM approach [8]. The linchpin of the RVM framework is the dynamical nature of the VED framed in the fundamental context of QFT in curved spacetime or in low-energy string theory. Appropriate renormalization in this context gets rid of the quartic mass terms $\sim m^4$ responsible for the fine tuning troubles, and as a result the VED becomes a smooth function of even powers of the Hubble rate [45–48]. This leads to a fairly good description of the cosmological data and helps easing the tensions [49, 50]. Worth noticing is also the phenomenological performance of the stringy version of the RVM [51]. All that said, we cannot exclude that the DE may be a composite fluid, a possibility which could further help in the task of alleviating these tensions. For this reason a good candidate is the aforementioned ‘ Λ XCDM model’ [42–44], a RVM-born model which was initially motivated as a possible cure for the cosmic coincidence problem. In it, we have two DE components: one is the running VED, $\rho_{\text{vac}} = \rho_{\text{vac}}(H)$, and the other is the mentioned X . As a matter of fact, the entity X need not be a fundamental field, as emphasized in [42]: it may just be due to particular terms in the effective action which mimic a dynamical DE component. In this sense, X can have phantom-like behavior without causing uproar at the theoretical level. Not only so, X may even display “phantom matter” (PM) behavior [42], namely an intriguing form of DE which, in stark contrast to the usual phantom DE, is characterized by a positive pressure ($p_X > 0$) at the expense of a negative energy density ($\rho_X < 0$). It is remarkable that there exists specific theoretical scenarios in the current literature which support the Λ XCDM structure with a PM-like component X . An example appears in the stringy RVM context [10, 11]. No less remarkable is the fact that the phenomenological performance attained by such a peculiar composite DE scenario surpasses by far that of the standard Λ CDM, as we shall shortly report. However, for the sake of simplicity, in this Letter we shall address a reduced version of the Λ XCDM, which we call the w XCDM model (not to be confused with the conventional w CDM parameterization), in which the additional X component of the Λ XCDM is kept intact, but on the other hand we mimic the running Λ with another dynamical component which we call Y . While the analysis within the full Λ XCDM will be presented elsewhere, we shall nonetheless demonstrate here that even the simplified w XCDM proves extremely efficient in dealing with the cosmological tensions, provided that the X component behaves as phantom matter. The information criteria applied to the results of our fitting analyses indeed bolster such a scenario as a most competitive one. The upshot is that we have a good theoretical framework to accommodate phantom matter, which proves phenomenologically optimal to quell the cosmological tensions and provides a far better global fit than the Λ CDM.

2 Composite dark energy

We next mention three related types of composite models of the DE: i) Λ XCDM, ii) w XCDM and iii) Λ_s CDM. As noted, model i) exists in different versions since long ago [42–44]; model ii) will be analyzed here for the first time, it constitutes a simplified version of model i) and embodies the PM feature. Finally, model iii) was recently analyzed in [40].

- i) Λ XCDM model. Its definition and comprehensive discussion, including the background cosmological solution, are provided in utmost detail in [42]. In addition, in [44] the corresponding cosmic perturbations equations are fully accounted for. Here we just present a very short qualitative description. Within the Λ XCDM, the cosmic fluid contains the usual matter energy density ρ_m and a composite DE sector made out of two components, one is the running vacuum energy density ρ_{vac} and the other is called X , with energy density ρ_X . The VED here is treated within the QFT framework of the RVM [45–48], in which $\rho_{\text{vac}} = \rho_{\text{vac}}(H)$ evolves with the expansion rate. In the current universe, such an evolution reads [8]:

$$\rho_{\text{vac}}(H) = \rho_{\text{vac}}^0 + \frac{3\nu_{\text{eff}}}{8\pi} (H^2 - H_0^2) m_{\text{Pl}}^2, \quad (1)$$

with ρ_{vac}^0 the current VED value, m_{Pl} the Planck mass and $|\nu_{\text{eff}}| \ll 1$ a small parameter which is formally computable in QFT, see the aforementioned papers. For $\nu_{\text{eff}} > 0$ the VED decreases with the expansion and hence the RVM mimics quintessence, whereas for $\nu_{\text{eff}} < 0$ the VED increases with the expansion and the RVM behaves effectively as phantom DE. The measured cosmological term is $\Lambda = 8\pi G\rho_{\text{vac}}$, and hence Λ also runs with H since $\rho_{\text{vac}} = \rho_{\text{vac}}(H)$. Such a running feature of the VED and Λ occurs in the Λ XCDM too, and in exactly the same form (1), but here we have also the dynamics of X and hence the cosmological solution of the model in terms of the redshift variable is considerably more complicated [42]. Besides, as recently demonstrated in the QFT context, ρ_{vac} has an EoS which departs from -1 [47], so the “modern version of the Λ XCDM model” has actually two nontrivial EoS parameters, one for the running VED and the other for X , which we call w_X . These are basic ingredients in our analysis, and for this reason the Λ XCDM fleshes out the theoretical basis inspiring the current work. However, the actual scenario which we will analyze here is model w XCDM (see below). It is simpler than the Λ XCDM but it has the same genetic ingredients. We will use it to emulate the basic properties of the latter. The analysis of the cosmic tensions within the full Λ XCDM framework is more demanding and will be presented in a separate work [52].

- ii) w XCDM model. In order to illustrate the possibilities of our composite DE scenario in connection with the cosmological tensions, herein we will use the w XCDM model, a reduced (skeleton) version of the Λ XCDM. The two models share the X component, but w XCDM mimics the running vacuum feature of Λ XCDM through another dynamical component Y (replacing Λ) and whose EoS w_Y can be different from -1 . This means that Y does not act as a rigid CC, Λ , which is fair enough since, as mentioned before, in the RVM context the EoS of the VED (hence of Λ) actually departs from -1 owing to quantum effects [47]. Thus, in the w XCDM, we have two DE components with potentially different EoS behaviors. Furthermore, as we will see in section 5, in the best-fit model the X component behaves phantom-like ($w_X \lesssim -1$) and the Y component behaves quintessence-like ($w_Y \gtrsim -1$). An important point is that X and Y do not act simultaneously: X acts first in the cosmic expansion, whilst Y acts subsequently. To be precise, X enters only above a transition redshift $z > z_t$ (fitted from the data) and Y enters below that redshift until the current time. No less crucial is the fact that the phantom-like component X actually behaves as PM, therefore with negative energy density ($\Omega_X = \rho_X/\rho_c < 0$) and positive pressure ($p_X > 0$), whereas for the Y component we have $\Omega_Y > 0$, $p_Y < 0$. Notice that the characteristic free parameters of model w XCDM are just (z_t, w_X, w_Y) . Indeed, the density parameters for the DE components are not free since e.g. the value of $\Omega_Y^0 \equiv \Omega_Y(z=0)$ depends on the fitting values

of $H_0, \omega_b, \omega_{\text{dm}}$ (cf. Table 1). In addition, the respective values of Ω_X and of Ω_Y immediately above and below z_t are assumed to be equal in absolute value. Thus, this means that $|\Omega_X(z)| = \Omega_Y(z)$ at $z = z_t$. This kind of assumption aims at reducing the number of parameters and is entirely similar to the one made in the $\Lambda_s\text{CDM}$ model, see point iii) below.

Last, but not least, we note that the existence of these two different phases of the DE separated by the redshift z_t is not just an ad hoc assumption since it is found in theoretical contexts such as the stringy RVM approach [11], which points to the existence of transitory domains or bubbles of PM whenever the universe is approaching a de Sitter epoch (see next sections for more elaboration).

- iii) $\Lambda_s\text{CDM}$ model. This is the model recently analyzed with considerable phenomenological success in [40]. Strictly speaking, it is not a composite model since only Λ is involved, although it enters with two signs and in this sense it is a composition of two phases of Λ separated also by a transition redshift z_t , which is the characteristic parameter of this model. It is assumed that at that point there is a sudden AdS-dS transition from $-\Lambda < 0$ in the upper redshift range to $+\Lambda > 0$ in the lower range, i.e. an abrupt change of sign of Λ at $z = z_t$, but keeping the same absolute value. We refer the reader to the quoted reference for more details.

For convenience, we shall simultaneously provide the fitting results for models ii) and iii) under the very same data sources. Together with the standard ΛCDM model, the simultaneous analysis of $\Lambda_s\text{CDM}$ will be useful as a benchmark for rating the performance of the phantom matter approach $w\text{XCDM}$ to the cosmological tensions. At the same time we will provide the results for the standard ΛCDM .

3 Phantom matter and the energy conditions of the cosmic fluids

Even though phantom matter was first proposed phenomenologically in the old composite cosmological model ΛXCDM [42–44], more recently it has been put forward on more formal grounds in [11], specifically within the context of the stringy RVM approach, see [10] for a review. Obviously, we need not provide technical details here and we refer the reader to the aforesaid references. However, we can at least describe the conceptual design of this picture. In a nutshell, it is the following: in a framework of a string-inspired cosmology with primordial gravitational waves and gravitational anomalies, which lead to dynamical inflation of RVM type without the need for ad hoc inflaton fields [10, 19], a crucial role is played by the fundamental axion field existing in the gravitational multiplet of string theory, viz. the Kalb-Ramond axion field $b(x)$, which couples to the gravitational Chern-Simons (gChS) term: $\sim b(x) R_{\mu\nu\rho\sigma} \tilde{R}^{\mu\nu\rho\sigma} \equiv b(x) R \tilde{R}$, where \tilde{R} denotes the dual of the Riemann tensor. The KR axion, when combined with the gChS contribution, obey together a peculiar equation of state $p = -\rho$ with negative energy density $\rho < 0$ (hence with positive pressure $p > 0$), which defines the ‘phantom vacuum’ [11]. This form of vacuum, however, is merely transitory until the gChS condensates $\langle R \tilde{R} \rangle$ become activated through the condensation of primordial gravitational waves (GW), thereby making possible a positive-definite vacuum state energy with effective cosmological ‘constant’ $\Lambda(H) \sim \langle b R \tilde{R} \rangle$. At this juncture, the total pressure and density already involve the combined effect from all the contributions, what makes possible a normal vacuum state with $p_{\text{total}} = -\rho_{\text{total}} < 0$, i.e. a standard de Sitter phase with positive density and negative pressure. The latter nevertheless may still be subdued to corrections owing to quantum effects. Interestingly enough, in such a framework the KR axion can be a candidate to Dark Matter, what provides an additional motivation for this cosmological picture since it could embrace the entire cosmic history.

Thus, a phantom-matter dominated era can be present in the early cosmic evolution near a de Sitter phase, but we should emphasize that it could also reflowerish in the late universe. As shown in [53–55], owing to the generation of chiral matter, which will dominate the universe at the exit from inflation, at large scales the universe can recover its FLRW background profile. This

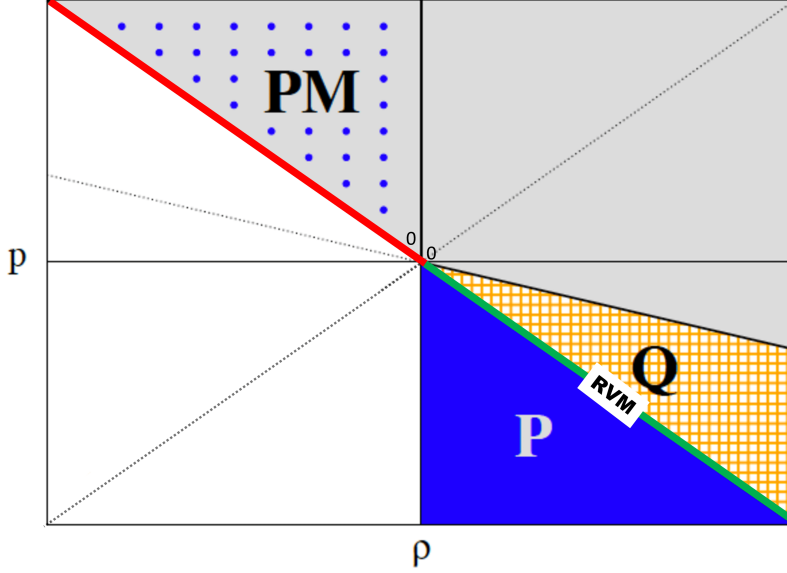


Figure 1: Energy conditions for the cosmic fluids. The quintessence (Q) region ($-1 < w < -1/3$ with $\rho > 0$, $p < 0$) is marked cross-hatched, and the conventional phantom region ($w \leq -1$ with $\rho > 0$, $p < 0$) is the blue sector indicated as P. The gray-dotted area corresponds to the peculiar “Phantom Matter” (PM) region: $w < -1$ with $\rho < 0$ and $p > 0$. Notice that PM satisfies the strong energy condition: $\rho + p \geq 0$, $\rho + 3p \geq 0$ (all of the gray area) but not the weak energy condition: $\rho \geq 0$, $\rho + p \geq 0$ (shaded area, except the P and PM sectors). The DE component X in our analysis behaves as PM, whereas the Y component behaves as quintessence. The EoS line $w = -1$ marks off the classical vacuum. The RVM fulfills this EoS only approximately near our time owing to quantum effects [47]. See also [42], and [11] for the modern developments on PM.

is because the chiral matter fields insure the cancellation of the gravitational anomalies during the FLRW regime, where they are indeed not observed as otherwise it would imply a glaring violation of general covariance. However, as soon as we are in the process of exiting the FLRW regime towards a new de Sitter era, we cannot exclude that in successive stages of the cosmic evolution the universe can be affected by the presence of lurking PM. The reason is that the chiral matter fields will get more and more diluted with the cosmic expansion and, then, owing to the incomplete cancellation of the gravitational anomalies, these may eventually re-surface near the current quasi-de Sitter era. It is therefore not inconceivable to think of the existence of phantom matter bubbles or domains tunneling now and then into our universe at relatively close redshift ranges before the ultimate de Sitter phase takes over. These bubbles of PM, being endowed with positive pressure $p > 0$, could obviously foster a larger rate of the structure formation, a fact which might explain the overproduction of large scale structures at unexpected places and times deep in our past. As we shall next show, this ideology provides an excellent framework for a fit to the overall cosmological data which proves to be (far) better than that of the standard Λ CDM model. We refer once more the reader to [11] and the review [10] for the details underlying the PM scenario supporting our proposal for solving the tensions. See also [56] and the recent developments [57, 58]. Here we have limited ourselves to a very succinct exposition of the theoretical background and in the rest of this work we focus on exploring the phenomenological implications.

Before closing this section and for the sake of a better contextualization of the PM option within the class of energy conditions, we show in Fig. 1 some of the most common possibilities for the EoS satisfied by the cosmic fluids. In it, we highlight the phantom matter (PM) region. As can be seen, it is very different from the usual phantom DE, it lies actually in its antipodes. These two phantom-like possibilities, both satisfying $w = -1$, are therefore dramatically different.

4 Data and numerical analysis

Leaving model i) for a separate study [52], in this work we constrain the DE models ii) and iii) described in section 2 making use of the following cosmological data sets:

- The full Planck 2018 CMB temperature, polarization and lensing likelihoods [4].
- The SNIa contained in the Pantheon+ compilation [59], calibrated with the cosmic distance ladder measurements of the SH0ES Team [60]. We refer to this data set as SNIa+SH0ES for short.
- 33 data points on $H(z)$ in the redshift range $z \in [0.07, 1.97]$ from cosmic chronometers (CCH) [61–70], see Appendix A of [71]. We employ the corresponding full covariance matrix, as described in [72].
- Transverse (aka angular or 2D) BAO data from Refs. [73–77]. This type of BAO data are claimed to be less subject to model-dependencies, since they are obtained without assuming any fiducial cosmology to convert angles and redshifts into distances to build the tracer map. These data points are extracted from the two-point angular correlation function or its Fourier transform. In anisotropic (or 3D) BAO analyses, instead, a fiducial cosmology is typically employed to construct the 3D map in redshift space, potentially introducing some model-dependence. Moreover, some studies have suggested that uncertainties may be underestimated by a factor of two in these analyses [78]. In contradistinction to the 3D BAO data, 2D BAO observations still give room for low-redshift solutions to the Hubble tension while respecting the constancy of the absolute magnitude of SNIa [37, 40].
- The data on large-scale structure at $z \lesssim 1.5$ from Refs. [79–89]. These are data points on the observable $f(z)\sigma_8(z)$, with $f(z) = -(1+z)d\ln\delta_m/dz$ the growth rate, $\delta_m = \delta\rho_m/\rho_m$ the matter density contrast, and $\sigma_8(z)$ the rms mass fluctuations at a scale $R_8 = 8h^{-1}$ Mpc, see Table 3 of [50]. These data points, though, are taken by the observational groups using a fiducial cosmology with $h \sim 0.67$, which translates into measurements at a characteristic scale of $R \sim 12$ Mpc. Here, in contrast, we adhere to the reasoning and practice of Refs. [22–24], and we treat these observations as data points on $f(z)\sigma_{12}(z)$, using a Fourier-transformed top-hat window function $W(kR_{12})$ in the computation of $\sigma_{12}(z)$. The advantage, as emphasized by these authors, is that the scale $R_{12} = 12$ Mpc is independent of the parameter h .

We compute all the cosmological observables using a modified version of the Einstein-Boltzmann code CLASS [90, 91], and explore and constrain the parameter space of the various models using the Metropolis-Hastings algorithm [92, 93] implemented in MontePython [94, 95]. The resulting Monte Carlo Markov chains are analyzed with the Python code GetDist [96]. Our main numerical results are presented in Table 1 and in the triangle plots of Figs. 2-3. Supplementary information on plots and tables is provided in the Appendix, which will be commented on in the main text.

In Table 1 we do not only list the mean of the various parameters, with their uncertainties and best-fit values, but also report the minimum values of χ^2 obtained for each model and the difference between the deviance (DIC) [97] and Akaike (AIC) [98] information criteria found between the composite DE models and Λ CDM, which we treat as our fundamental benchmark model. These differences read $\Delta\text{DIC} \equiv \text{DIC}_{\Lambda\text{CDM}} - \text{DIC}_i$ and $\Delta\text{AIC} \equiv \text{AIC}_{\Lambda\text{CDM}} - \text{AIC}_i$, respectively, with i referring to w XCDM or Λ_s CDM. Both criteria penalize the use of additional parameters and can be regarded as a rigorous mathematical implementation of Occam’s razor. The DIC is defined as

$$\text{DIC} = \chi^2(\bar{\theta}) + 2p_D, \quad (2)$$

Parameter	Λ CDM	w XCDM	Λ_s CDM
ω_b	0.02281 ± 0.00014 (0.02278)	0.02241 ± 0.00013 (0.02260)	$0.02236^{+0.00016}_{-0.00018}$ (0.02232)
ω_{dm}	0.1153 ± 0.0009 (0.1148)	0.1199 ± 0.0010 (0.1196)	$0.1205^{+0.0015}_{-0.0016}$ (0.1216)
$\ln(10^{10} A_s)$	$3.066^{+0.016}_{-0.018}$ (3.080)	3.037 ± 0.014 (3.034)	$3.036^{+0.015}_{-0.016}$ (3.030)
τ	$0.069^{+0.008}_{-0.010}$ (0.076)	0.051 ± 0.008 (0.048)	$0.050^{+0.008}_{-0.009}$ (0.046)
n_s	0.978 ± 0.004 (0.981)	0.967 ± 0.004 (0.969)	$0.966^{+0.004}_{-0.005}$ (0.961)
H_0 [km/s/Mpc]	$69.82^{+0.41}_{-0.44}$ (70.05)	$72.75^{+0.57}_{-0.71}$ (72.36)	$72.24^{+0.99}_{-0.75}$ (73.82)
z_t	—	$1.46^{+0.02}_{-0.01}$ (1.47)	$1.61^{+0.22}_{-0.18}$ (1.47)
w_X	—	$-1.16^{+0.13}_{-0.16}$ (-1.16)	—
w_Y	—	-0.90 ± 0.03 (-0.88)	—
Ω_m^0	0.283 ± 0.005 (0.280)	0.269 ± 0.005 (0.272)	0.267 ± 0.005 (0.264)
M	$-19.372^{+0.011}_{-0.012}$ (-19.362)	$-19.273^{+0.015}_{-0.016}$ (-19.282)	$-19.278^{+0.026}_{-0.020}$ (-19.261)
σ_{12}	0.780 ± 0.007 (0.884)	0.776 ± 0.007 (0.772)	$0.782^{+0.007}_{-0.006}$ (0.784)
χ_{min}^2	4166.76	4107.62	4120.04
ΔDIC	—	57.94	40.16
ΔAIC	—	53.14	44.72

Table 1: Mean values and uncertainties at 68% CL obtained with the full data set CMB+CCH+SNia+SH0ES+BAO+ $f\sigma_{12}$. We show the best-fit values in brackets. We use the standard notations for the Λ CDM parameters. In the last three lines, we display the values of the minimum χ^2 , ΔDIC and ΔAIC , as defined in Eqs. (2) and (3), respectively. Positive values of ΔDIC and ΔAIC denote preference of the new models over the Λ CDM. As can be seen, the preference is extraordinarily high.

with $p_D = \overline{\chi^2} - \chi^2(\bar{\theta})$ the effective number of parameters in the model, $\overline{\chi^2}$ the mean value of χ^2 , and $\bar{\theta}$ the mean of the parameters that are left free in the Monte Carlo analysis. Similarly, AIC is defined as

$$\text{AIC} = \chi_{\text{min}}^2 + 2n_p, \quad (3)$$

with n_p the number of parameters entering the fit. With our definition, a positive difference of these information criteria implies that the composite DE models perform better than the Λ CDM, whereas negative differences imply just the opposite. According to the usual jargon of the information criteria, if $0 \leq \Delta\text{DIC} < 2$ it is said that one finds *weak evidence* in favor of the new model under test (in this case, the composite DE models under scrutiny), as compared to the standard model. If $2 \leq \Delta\text{DIC} < 6$ we speak, instead, of *positive evidence*. If $6 \leq \Delta\text{DIC} < 10$, there is *strong evidence* in favor of the composite DE models, whilst if $\Delta\text{DIC} > 10$ we can conclude that there is *very strong evidence* supporting the new model or models against the standard Λ CDM. An analogous consideration can be made using AIC, of course. DIC is considered to be a more

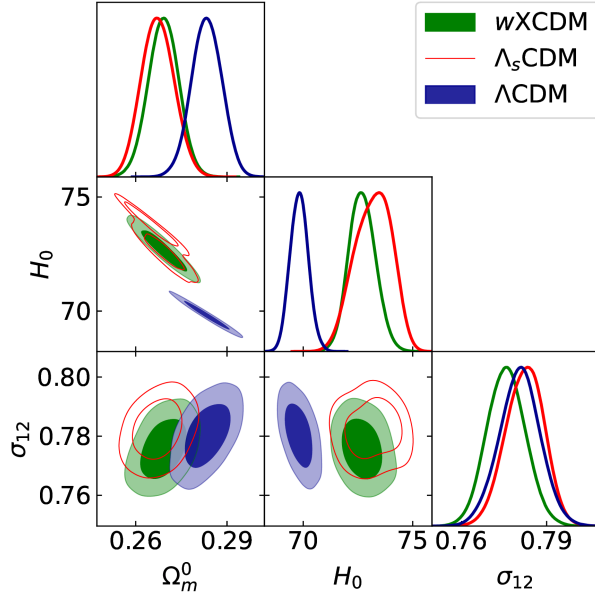


Figure 2: Contour plots at 68% and 95% CL and the corresponding one-dimensional posterior distributions for some of the parameters that are relevant in the discussion of the cosmological tensions, for all the models under study. H_0 is given in km/s/Mpc. The complete triangle plot is presented in Fig. 4 of the Appendix.

accurate information criterion, since it incorporates the information encapsulated in the full Markov chains. However, for the sake of generality and to explicitly show the consistency between these two criteria, we display the results obtained from both criteria in our Table 1.

5 Discussion

As we have mentioned, bubbles of PM are connected with the process of attaining the de Sitter (dS) era both in the early and the late universe. During the transit from the provisional phantom vacuum into the true and stable (dS) vacuum, the PM bubbles being tunneled in the late universe are characterized by positive pressure and hence offer a fertile field for the growing of unsuspected structures. This mechanism, therefore, provides a tantalizing theoretical framework capable of explaining physically the appearance of a late time AdS epoch (or epochs) before the usual dS epoch is eventually attained³. In point of fact, we do not expect that these PM bubbles are perfect AdS phases (nor that the subsequent stage is necessarily characterized by a rigid $\Lambda > 0$) and for this reason we have left the EoS parameter w_X as a free parameter, whose fitted value is $w_X \simeq -1.16$ (cf. Table 1). Since the bubble is transitory, the ensuing DE phase below z_t carries another EoS which we fit it to be quintessence-like: $w_Y \simeq -0.90$ (see Table 1). We have performed a comparative fit of the w XCDM and Λ_s CDM scenarios using the same data sets and have found a significantly better fit for the PM scenario, as shown in Table 1.

The PM phase (or phases) with negative energy density and positive pressure are left behind during the cosmic evolution at relatively large redshifts of order $1 - 10$, and in these places they can leave a sort of oasis of large scale structures, whereas the consecutive evolution (closer to our time) flips into the quintessence regime. Although we have used an abrupt θ -function behavior to connect the two EoS regimes, in practice the process is continuous since the Chern-Simons condensates eventually dominate and restore the normal vacuum phase with positive energy. To

³This is in contradistinction to the alternative Λ_s CDM scenario analyzed in [40], although theoretical attempts at justifying it have appeared recently [99–101].

better understand how the PM bubbles with positive pressure enhance the formation of large (unsuspected) structures in the relatively distant past, it is useful to analyze the equation for the matter density contrast in the presence of PM. We shall not provide details of the perturbations equations here (see [52]), but we wish at least to highlight this important aspect associated to the presence of PM in a more quantitative way. Before the transition at z_t (i.e. at $z > z_t$), the equation for δ_m reads

$$\delta_m'' + \frac{3}{2a} (1 - \Omega_X(a)w_X) \delta_m' - \frac{3}{2a^2} (1 - \Omega_X(a)) \delta_m = 0, \quad (4)$$

with the primes denoting derivatives with respect to the scale factor. PM has negative energy density ($\Omega_X < 0$) and positive pressure (due to $w_X < -1 < 0$) and, therefore, it induces a decrease of the friction term and an increase of the Poisson term in Eq. (4). Both effects are in harmony and bring about, given some fixed initial conditions, an enhancement of the structure formation processes in the PM bubbles. Notice that this would not occur for ordinary phantom DE or quintessence (cf. Fig. 1), for which the friction term gets enhanced and the Poisson term suppressed, i.e. just opposite to PM.

Moreover, because the energy of the X entity is negative (and non-negligible at high redshift, in absolute value), this enforces a higher value of the expansion rate H in the quintessence stage in order to preserve the angular diameter distance to the last scattering surface, which is essentially fixed by the precise measurement of θ_* (the angular size of sound horizon) by Planck [4] and the standard physics before recombination [37]. This explains why H_0 is found larger than in the Λ CDM in our PM scenario. Quantitatively, our value of H_0 (cf. Table 1) is in full agreement with that of SH0ES ($H_0 = 73.04 \pm 1.04$ km/s/Mpc) [60] to within $\lesssim 0.25\sigma$. The Hubble tension is therefore virtually washed out, also when it is formulated in terms of the absolute magnitude of SNIa: our fitted value of M and that of SH0ES ($M = 19.253 \pm 0.027$ mag) differ by only $\sim 0.6\sigma$. At the same time the rate of LSS formation becomes suppressed below $z_t \sim 1.5$ during the quintessence-like regime, as explained above, which is in accordance with the observations. In Table 1 and, more graphically, in Fig. 2, we can see that the amplitude of the power spectrum at linear scales that is preferred by the data is pretty similar in all the models under study. Indeed, in all cases we find values of $\sigma_{12} \sim 0.78$. However, at a finer level, Table 2 in the Appendix tells us that the w XCDM is able to describe better the LSS data than Λ CDM, what means that the former model is able to produce lower values of $f(z)\sigma_{12}(z)$ and, hence, of $f(z)$ since σ_{12} remains stable in the various models. This can again be understood by looking at the equation for the density contrast, whose form at $z < z_t$ is identical to Eq. (4), but with the replacements $\Omega_X \rightarrow \Omega_Y$ and $w_X \rightarrow w_Y$,

$$\delta_m'' + \frac{3}{2a} (1 - \Omega_Y(a)w_Y) \delta_m' - \frac{3}{2a^2} (1 - \Omega_Y(a)) \delta_m = 0. \quad (5)$$

It is clear from Fig. 2 that the values of the matter density parameter $\Omega_m^0 = \Omega_m(a=1)$ in the w XCDM are a way smaller than in Λ CDM. This obviously translates into larger values of $\Omega_Y(a) > 0$ (higher than Ω_Λ^0 in the Λ CDM), which makes matter fluctuations to grow less efficiently in our model after the transition (at $z < z_t$), obviously a welcome feature. As previously mentioned, despite the presence of PM in the past, the value of σ_{12} in w XCDM is not significantly different ($\sim 0.4\sigma$) from that of Λ CDM. This is due to the slower increase of matter fluctuations in the late-time universe and the smaller value of the amplitude of primordial fluctuations (A_s) found in w XCDM, which somehow compensate for the previous effects, cf. again Table 1 and Fig. 4.

From our numerical analysis we can see that both models w XCDM and Λ_s CDM offer a dramatic reduction of the cosmological tensions. This is apparent from Table 1. One could say that the Hubble and growth tensions disappear in these models. However, there are also important quantitative (and conceptual) differences between them. In terms of the information criteria, we

find that the two models $w\Lambda\text{CDM}$ and $\Lambda_s\text{CDM}$ are very strongly preferred over ΛCDM . Numerically, however, the $w\Lambda\text{CDM}$ solution provides a significantly better global fit. For this model we find $\Delta\text{DIC}, \Delta\text{AIC} \gtrsim 55$, whereas for $\Lambda_s\text{CDM}$ we obtain $\Delta\text{DIC}, \Delta\text{AIC} \gtrsim 40$. The difference of 15 units is quite substantive and indicates (in the common parlance of the information criteria) that there is very strong evidence that model $w\Lambda\text{CDM}$ is preferred over model $\Lambda_s\text{CDM}$ (for the same data). Worth noticing is also the fact that our own results for $\Lambda_s\text{CDM}$ agree with those originally reported in [40], despite the existing differences in the data sets employed in the two analyses. Apart from our using data on CCH, which were not considered in [40], we employ data on $f(z)\sigma_{12}(z)$ instead of the weak lensing (WL) data from KiDS. We do not use WL data in our analysis in order not to compromise the computation of the non-linear matter power spectrum, which might not be sufficiently well under control in the models under study. Our fitting results, though, are completely consistent with theirs, leading also to similar values of $S_8 \sim 0.78$ (as we have checked), the latter being a more natural LSS parameter in the context of WL analyses, but not in our approach.

Perhaps the most remarkable outcome of our analysis is that in the light of the overall fit quality of our results leading to such an outstanding support to the composite DE models from the information criteria, it should be fair to conclude that the standard ΛCDM model appears to be comparatively ruled out at a very high confidence level. Let us analyze the degree of impact from each data source on the previous statement. It can be inferred from Table 2 in the Appendix, where a detailed breakdown of the different contributions is reckoned. The angular/transversal BAO data certainly contributes in a significant way, as could be expected from the analysis of [37]. However, it is by no means the leading contribution, as it is responsible for roughly $\sim 18\%$ of the success. A close inspection of the mentioned table shows that the composite DE models beat actually the ΛCDM in every single observable, not only in those driving the tensions. Particularly noticeable is the sizeable impact from such a solid asset of basic data as the CMB and SNIa+SH0ES observations, which are responsible for about 70% of our successful fitting result, whereas the influence from LSS data is less than 10%; and, finally, that of CCH is marginal (a few percent). The bulk of the successful fit, therefore, hinges upon the most fundamental cosmological data, which is truly remarkable. The ΛCDM is not only unable to explain the large values of H_0 measured by SH0ES or to further slow down the structure formation rate at low redshift, but it also introduces other tensions, e.g. with the value of the (reduced) cosmological matter parameter $\omega_m = \omega_b + \omega_{\text{dm}}$ that is preferred by the Planck data in models which assume standard model physics before the decoupling of the CMB photons, $\omega_m = 0.142 \pm 0.001$ [4]. The latter is fully consistent with the value obtained in the $w\Lambda\text{CDM}$ ($\omega_m = 0.142 \pm 0.001$), but differs by 2.8σ with the one inferred in the standard ΛCDM ($\omega_m = 0.138 \pm 0.001$).

We should emphasize that the outperformance of the composite models under study as compared to the ΛCDM is obtained after duly penalizing the use of extra parameters in them. This is of course implemented automatically by the information criteria, as explained above. Thus, for the $\Lambda_s\text{CDM}$ there is the transition redshift z_t as a new parameter with respect to the ΛCDM , whereas for the $w\Lambda\text{CDM}$ we have, in addition, the two EoS parameters w_X and w_Y for the two phases of the DE. Despite the presence of these extra parameters, Occam's razor (formalized through the verdict of the information criteria) still bestows exceptional preference for the composite models over the concordance model. This is the first important conclusion of our analysis, which suggests that the composite nature of the DE could be a fact. The second, is that the relative differences between the two composite models under scrutiny, namely $\text{DIC}_{\Lambda_s\text{CDM}} - \text{DIC}_{w\Lambda\text{CDM}} = 17.78$ and $\text{AIC}_{\Lambda_s\text{CDM}} - \text{AIC}_{w\Lambda\text{CDM}} = 8.42$, clearly point to a rather keen preference for $w\Lambda\text{CDM}$ over $\Lambda_s\text{CDM}$ under the same data.

Focusing now on the $w\Lambda\text{CDM}$ parameters, in Fig. 3 we show the constraints obtained in the EoS plane w_Y - w_X , which involves two of the characteristic new parameters of the $w\Lambda\text{CDM}$

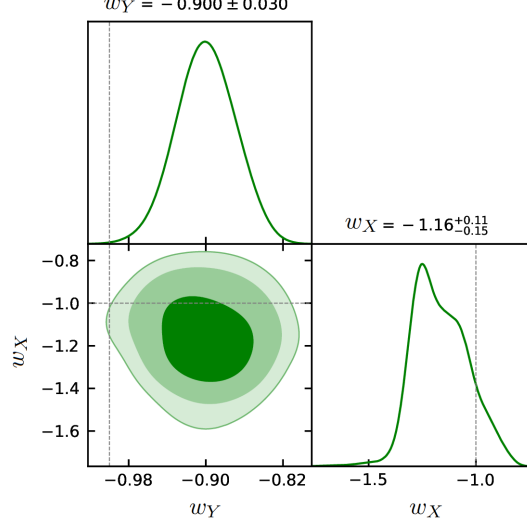


Figure 3: Confidence regions in the $w_Y - w_X$ plane of the $wXCDM$ model, and the corresponding one-dimensional posterior distributions. The dotted lines are set at $w_Y = -1$ and $w_X = -1$. The intersection of the horizontal and vertical lines in the contour plot corresponds to the Λ_sCDM model, which falls $\gtrsim 3\sigma$ away from the preferred region of the $wXCDM$. See the main text for further comments.

model (the third one being z_t , shared with Λ_sCDM). The central value of $w_X = -1.16$ falls in the phantom region (in fact, PM region since $\Omega_X < 0$) but is compatible with -1 at $\sim 1\sigma$ CL. There is, in contrast, a non-negligible ($\sim 3.3\sigma$) preference for a quintessence-like evolution of the DE for the low redshift range nearer to our time ($z < z_t$): $w_Y = -0.90 \pm 0.03$ (see also Fig. 3). The preference that we find for quintessence-like behavior in this region can be contrasted with the situation in the Λ_sCDM , where a simple Λ -term is assumed below the transition redshift (also above that redshift, with $\Lambda \rightarrow -\Lambda$). Now the fact that our fit with model $wXCDM$ proves significantly better than with model Λ_sCDM (as commented above) suggests that indeed the quintessence option in the low redshift range is strongly preferred. Our result aligns perfectly well with the one obtained from the analysis of the Pantheon+ data in the context of the flat $wCDM$ parametrization [59], which showed that SNIa data alone lead to an EoS parameter $w = -0.89 \pm 0.13$ after marginalizing over Ω_m^0 . This marginalized result, though, is still compatible with a CC ($w = -1$). To explain why in our case is more focused on the quintessence domain, let us note that for $wXCDM$ we find a tight constraint on the matter density parameter, strongly favoring the region of small values, $\Omega_m^0 = 0.269 \pm 0.005$. This is induced by two facts: (i) CMB prefers values of $\omega_m \sim 0.142$ in models with standard pre-recombination physics; and (ii) the large values of $H_0 \sim 73$ km/s/Mpc measured by SH0ES. Combining the aforementioned tight constraint on Ω_m^0 with the constraints in the $w - \Omega_m^0$ plane obtained for the $wCDM$ from the analysis of the Pantheon+ data alone (cf. the contours in cyan of Fig. 9 of [59]) we can break the existing degeneracy in that plane and explain the $\gtrsim 3\sigma$ evidence for quintessence DE that we find within the $wXCDM$ for the low redshift range. We point out that for the conventional $wCDM$ parameterization such low values of Ω_m^0 are not favored by Planck, since they are in tension with the angular diameter distance to the last scattering surface, see again Fig. 9 of [59]. Remarkably, this problem can be fully averted in the $wXCDM$ model owing precisely to the presence of PM in the high redshift stretch $z > z_t$, which compensates for the decrease of the contribution to the angular diameter distance in the low redshift domain. On the other hand, in the Λ_sCDM case we also find similar low values of Ω_m^0 , but to connect our $wXCDM$ with this model we have to set w_Y to -1 (rigid CC), so the model falls outside the 3σ region obtained with $wCDM$ using only SNIa data [59]. This issue is also solved in the $wXCDM$ and explains the improvement found with respect to the Λ_sCDM model. The full 5-year data set of high-

redshift SNIa from the Dark Energy Survey [102] and the Union3 SNIa compilation [103] will most likely increase the aforesaid signal, since they also find constraints in the region of interest, which read $(\Omega_m^0, w) = (0.264_{-0.096}^{+0.074}, -0.80_{-0.16}^{+0.14})$ and $(\Omega_m^0, w) = (0.244_{-0.128}^{+0.092}, -0.735_{-0.191}^{+0.169})$, respectively. Hence, it will be of utmost importance to study the impact of these data sets once they become publicly available. In addition, our fitting results for w XCDM are compatible at roughly $\sim 1\sigma$ with those recently reported by DESI using the w CDM parametrization [13]. Although two of the twelve DESI BAO data points (specifically those obtained with Ly- α quasars (QSO) at $z_{\text{eff}} = 2.33$) lie outside the quintessence region identified in our w XCDM model, the bulk of the DESI points lie below $z = 1.5$. The exclusion of the Ly- α QSO data points in their fitting analysis might even improve further the compatibility with our findings. Additionally, since the DESI data are derived from 3D BAO, exploring future angular BAO data from DESI (if available) and comparing them with the 3D BAO data would be an interesting avenue for further research.

6 Conclusions

In this Letter, we have addressed a possible solution to the cosmological tensions within a simplified version of the old existing Λ XCDM framework [42–44], which was born in the theoretical arena of the RVM – see [8,9] and references therein. Our modern approach benefits from the new theoretical developments in the context of the stringy version of the running vacuum model (StRVM) [10,11]. The entity X that is involved in the Λ XCDM need not be a fundamental field but can display a phantom matter (PM) behaviour, which in the StRVM is predicted to appear in the transit to the de Sitter phase. The PM regime is, therefore, only transitory and acts as a temporary stage with negative energy and positive pressure. It can be a pure anti-de Sitter (AdS) phase but in general its EoS w_X is not necessarily -1 , although it must satisfy $w_X \lesssim -1$. While in this work we have contented ourselves with a simplified version of the full Λ XCDM, which we have called the w XCDM, the analysis of the full model (in which the VED is running) will be presented elsewhere [52]. Using provisionally the w XCDM model, we find that the PM phase shows up above a transition redshift $z_t \simeq 1.5$ (cf. Table 1). For $z > z_t$ the PM behavior is rapidly washed out since its energy density fraction becomes smaller and smaller in the past. And, on the other hand, its effect towards our time ($z < z_t$) becomes erased by the progressive appearance of the Chern-Simons condensates, which will finally establish a steady $\Lambda = \text{const.} > 0$ regime [11]. For this reason, in practice the appearance of a PM phase is confined to a bubble of spacetime, which is left behind. However, in that space and time new structures can emerge, which are completely unsuspected in the context of the standard model. The PM bubbles which are met within the stringy RVM formulation originate as a result of a “phantom vacuum” phase which emerges in the universe when the expansion heads towards the next de Sitter epoch. While the implications of this fact for the early universe were considered previously [11], here we have extended this phenomenon to the late universe. In both cases the PM bubbles are evanescent, in that they are not carried forward in time and only occur as tunneling attempts to establish the phantom vacuum [11] $p = -\rho > 0$. Below the transition redshift, the PM phase ceases to occur and the field Y (viz. the would-be running VED in the full Λ XCDM [42]) takes its turn with an effective EoS which is found to be of quintessence type ($w_Y \gtrsim -1$) at $\sim 3.3\sigma$ CL. As a matter of fact, this is the effective form of DE that is expected in our most recent past ($z < 1.5$) within w XCDM, although from a more fundamental level it could just be running vacuum energy with $\nu_{\text{eff}} > 0$ in the full Λ XCDM model, see Eq. (1). The observed DE should thereupon be dynamical, and this important conclusion is in stark contrast with the alternative Λ_s CDM scheme analyzed in [40], in which below the transition redshift there is a rigid and positive cosmological term $\Lambda = \text{const.}$. Actually, no possible time dynamics for the DE is possible in the Λ_s CDM, neither above nor below z_t . On this account, the result from w XCDM looks more consistent with the first data release by

DESI [13], which suggests dynamical DE.

All in all, model w XCDM offers not only a significantly better quality fit than model Λ_s CDM, but at the same time does provide a richer conceptual framework for our understanding of the physical phenomena that may be involved. In the Λ_s CDM approach, no obvious physical explanation is provided for the AdS-dS transition nor for its single occurrence precisely near our time. In the w XCDM, instead, the formation of a PM bubble is induced by quantum fluctuations associated to the nearing of the universe towards a de Sitter phase. The phenomenon need not be unique: the bubbles of PM could well be operating more than once at earlier times on the same physical grounds, what would trigger an anomalous outgrowth of structures at even higher redshifts, say in the range $z \sim 5 - 10$. This might explain the appearance of the large scale structures recently spotted at unusually high redshifts by the JWST mission [30, 104, 105]. Such LSS ‘anomalies’, which find no explanation in the Λ CDM, might also be described within the current proposal since they can be conceived as being the earliest bubbles of PM popping up in the late universe, corresponding probably to the first tunneling attempts anticipating the eventual dS phase near our time. This is reasonable given the fact that the tunneling process towards the final de Sitter era should be gradual, exactly as in the early universe [11]. It is encouraging to realize that the physics involved in the PM scenario presented here for the solution to the cosmological tensions may ultimately stem from quantum vacuum phenomena, what gives real hope for eventually being able to achieve a deeper understanding of the entire cosmological evolution of the universe in the context of fundamental physics.

Acknowledgments This work is partially supported by grants PID2022-136224NB-C21 and PID2019-105614GB-C21, from MCIN/AEI/10.13039/501100011033. AGV is funded by “la Caixa” Foundation (ID 100010434) and the European Union’s Horizon 2020 research and innovation programme under the Marie Skłodowska-Curie grant agreement No 847648, with fellowship code LCF/BQ/PI21/11830027. JSP is funded also by 2021-SGR-249 (Generalitat de Catalunya) and CEX2019-000918-M (ICCUB, Barcelona). Both of us acknowledge networking support by the COST Association Action CA21136 “*Addressing observational tensions in cosmology with systematics and fundamental physics (CosmoVerse)*”.

Appendix: Full triangle plot and breakdown of χ^2_{\min} contributions

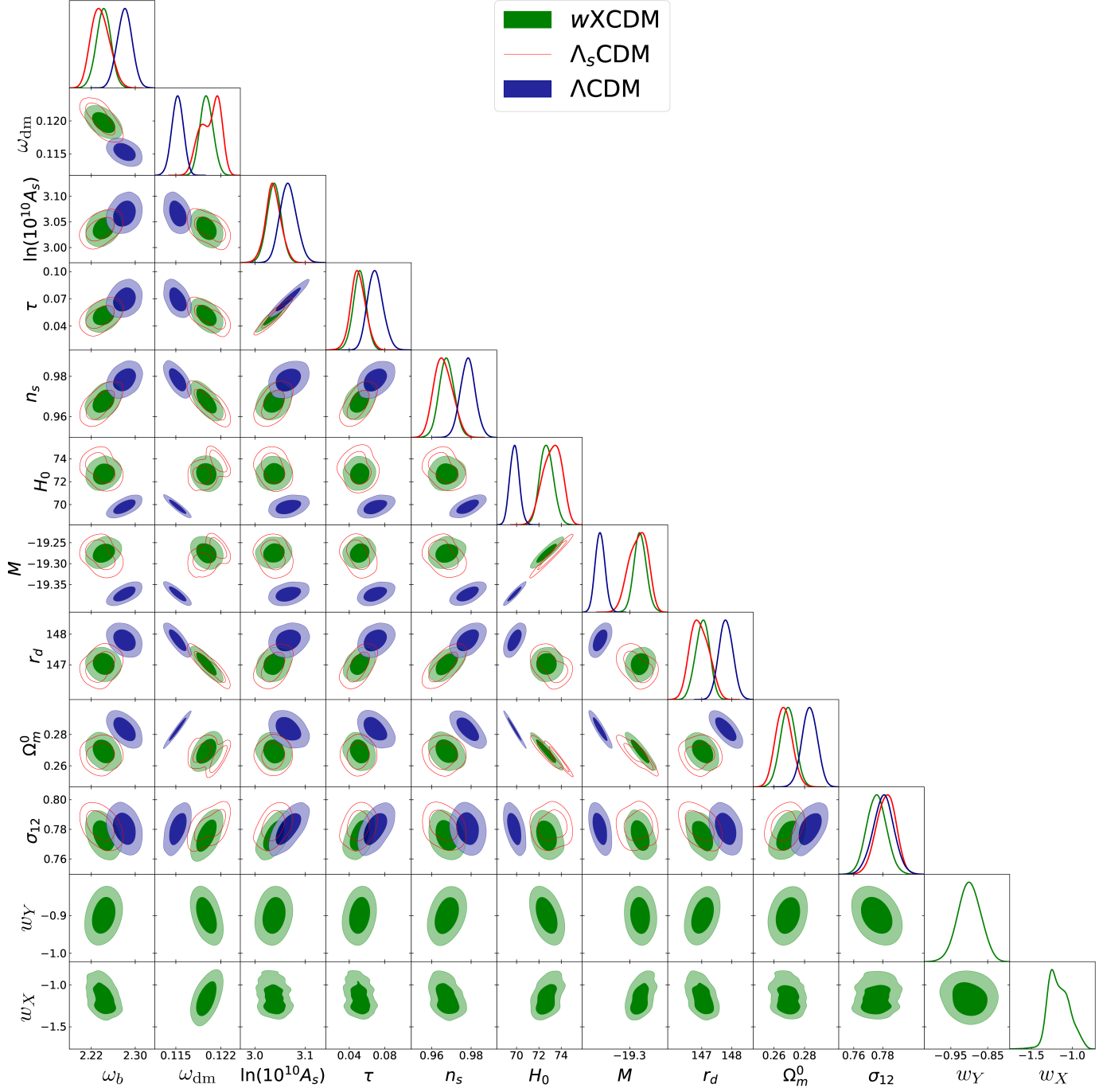


Figure 4: Full triangle plot for the various models studied in this paper. We show the constraints at 68% and 95% CL in all the relevant planes of the parameter spaces, together with the individual one-dimensional posterior distributions. H_0 is given in km/s/Mpc.

χ_i^2	Λ CDM	w XCDM	Λ_s CDM
$\chi_{\text{Planck_highL_TTTEEE}}^2$	2365.09	2350.78	2350.81
$\chi_{\text{Planck_lowL_EE}}^2$	404.20	395.91	396.07
$\chi_{\text{Planck_lowL_TT}}^2$	21.34	25.21	27.80
$\chi_{\text{Planck_lens}}^2$	10.77	9.31	10.74
χ_{CMB}^2	2801.40	2781.21	2785.42
$\chi_{\text{Pantheon+SH0ES}}^2$	1312.83	1290.11	1302.21
χ_{BAO}^2	23.87	13.27	13.80
$\chi_{f\sigma_{12}}^2$	15.99	12.68	9.41
χ_{CCH}^2	12.67	10.52	10.20
χ_{min}^2	4166.76	4107.62	4120.04

Table 2: Individual χ_i^2 contributing to χ_{min}^2 , obtained in the fitting analyses for the various models with CMB+CCH+SNIa+SH0ES+BAO+ $f\sigma_{12}$. χ_{CMB}^2 contains the total CMB contribution, i.e. it is the sum of all the Planck χ_i^2 , which we list in the upper half of the table.

References

- [1] P. J. E. Peebles, *Principles of physical cosmology*. Princeton University Press, 1993.
- [2] M. S. Turner, “The Road to Precision Cosmology,” *Annu. Rev. Nucl. Part. Sci.* 2022. 72:1–35. arXiv:2201.04741.
- [3] P. A. R. Ade *et al.*, “Planck 2015 results. XIII. Cosmological parameters,” *Astron. Astrophys.*, vol. 594, p. A13, 2016. arXiv:1502.01589.
- [4] N. Aghanim *et al.*, “Planck 2018 results. VI. Cosmological parameters,” *Astron. Astrophys.*, vol. 641, p. A6, 2020. [Erratum: *Astron. Astrophys.* 652, C4 (2021)]. arXiv:1807.06209.
- [5] S. Weinberg, “The Cosmological Constant Problem,” *Rev. Mod. Phys.*, vol. 61, pp. 1–23, 1989.
- [6] P. J. E. Peebles and B. Ratra, “The Cosmological Constant and Dark Energy,” *Rev. Mod. Phys.*, vol. 75, pp. 559–606, 2003. astro-ph/0207347.
- [7] T. Padmanabhan, “Cosmological constant: The Weight of the vacuum,” *Phys. Rept.*, vol. 380, pp. 235–320, 2003. hep-th/0212290.
- [8] J. Solà Peracaula, “The cosmological constant problem and running vacuum in the expanding universe,” *Phil. Trans. Roy. Soc. Lond. A*, vol. 380, p. 20210182, 2022. arXiv:2203.13757.
- [9] J. Solà, “Cosmological constant and vacuum energy: old and new ideas,” *J. Phys. Conf. Ser.*, vol. 453, p. 012015, 2013. arXiv:1306.1527.
- [10] N. E. Mavromatos and J. Solà Peracaula, “Stringy-running-vacuum-model inflation: from primordial gravitational waves and stiff axion matter to dynamical dark energy,” *Eur. Phys. J. ST*, vol. 230, no. 9, pp. 2077–2110, 2021. arXiv:2012.07971.
- [11] N. E. Mavromatos and J. Solà Peracaula, “Inflationary physics and trans-Planckian conjecture in the stringy running vacuum model: from the phantom vacuum to the true vacuum,” *Eur. Phys. J. Plus*, vol. 136, no. 11, p. 1152, 2021. arXiv:2105.02659.
- [12] O. Avsajanishvili *et al.*, “Observational Constraints on Dynamical Dark Energy Models,” *Universe*, vol. 10, no. 3, p. 122, 2024, arXiv:2310.16911.
- [13] A. G. Adame *et al.*, “DESI 2024 VI: Cosmological Constraints from the Measurements of Baryon Acoustic Oscillations,” arXiv:2404.03002.
- [14] J. Solà, A. Gómez-Valent, and J. de Cruz Pérez, “Hints of dynamical vacuum energy in the expanding Universe,” *Astrophys. J.*, vol. 811, p. L14, 2015. arXiv:1506.05793.
- [15] J. Solà, A. Gómez-Valent, and J. de Cruz Pérez, “First evidence of running cosmic vacuum: challenging the concordance model,” *Astrophys. J.*, vol. 836, no. 1, p. 43, 2017. arXiv:1602.02103.
- [16] J. Solà Peracaula, A. Gómez-Valent, and J. de Cruz Pérez, “The H_0 tension in light of vacuum dynamics in the Universe,” *Phys. Lett.*, vol. B774, pp. 317–324, 2017. arXiv:1705.06723.
- [17] J. Solà Peracaula, J. de Cruz Pérez, and A. Gómez-Valent, “Dynamical dark energy vs. $\Lambda = \text{const}$ in light of observations,” *EPL*, vol. 121, no. 3, p. 39001, 2018. arXiv:1606.00450.

- [18] J. Solà Peracaula, J. de Cruz Pérez, and A. Gómez-Valent, “Possible signals of vacuum dynamics in the Universe,” *Mon. Not. Roy. Astron. Soc.*, vol. 478, no. 4, pp. 4357–4373, arXiv:1703.08218.
- [19] J. Solà and A. Gómez-Valent, “The $\bar{\Lambda}$ CDM cosmology: From inflation to dark energy through running Λ ,” *Int. J. Mod. Phys. D*, vol. 24, p. 1541003, 2015, arXiv:1501.03832.
- [20] G.-B. Zhao *et al.*, “Dynamical dark energy in light of the latest observations,” *Nat. Astron.*, vol. 1, no. 9, pp. 627–632, 2017. arXiv:1701.08165.
- [21] J. Solà Peracaula, A. Gómez-Valent, and J. de Cruz Pérez, “Signs of Dynamical Dark Energy in Current Observations,” *Phys. Dark Univ.*, vol. 25, p. 100311, 2019. arXiv:1811.03505.
- [22] A. G. Sánchez, “Arguments against using h^{-1} Mpc units in observational cosmology,” *Phys. Rev. D*, vol. 102, no. 12, p. 123511, 2020. arXiv:2002.07829.
- [23] A. Semenaite *et al.*, “Cosmological implications of the full shape of anisotropic clustering measurements in BOSS and eBOSS,” *Mon. Not. Roy. Astron. Soc.*, vol. 512, no. 4, pp. 5657–5670, 2022. arXiv:2111.03156.
- [24] A. Semenaite *et al.*, “Beyond Λ CDM constraints from the full shape clustering measurements from BOSS and eBOSS,” *Mon. Not. Roy. Astron. Soc.*, vol. 521, no. 4, pp. 5013–5025, 2023. arXiv:2210.07304.
- [25] E. Di Valentino *et al.*, “Snowmass2021 - Letter of interest cosmology intertwined II: The hubble constant tension,” *Astropart. Phys.*, vol. 131, p. 102605, 2021. arXiv:2008.11284.
- [26] E. Di Valentino *et al.*, “Cosmology Intertwined III: $f\sigma_8$ and S_8 ,” *Astropart. Phys.*, vol. 131, p. 102604, 2021. arXiv:2008.11285.
- [27] L. Perivolaropoulos and F. Skara, “Challenges for Λ CDM: An update,” *New Astron. Rev.*, vol. 95, p. 101659, 2022. arXiv:2105.05208.
- [28] E. Abdalla *et al.*, “Cosmology intertwined: A review of the particle physics, astrophysics, and cosmology associated with the cosmological tensions and anomalies,” *JHEAp*, vol. 34, pp. 49–211, 2022. arXiv:2203.06142.
- [29] J. P. Gardner *et al.*, “The James Webb Space Telescope,” *Space Sci. Rev.*, vol. 123, p. 485, 2006. astro-ph/0606175.
- [30] I. Labbé *et al.*, “A population of red candidate massive galaxies ~ 600 Myr after the Big Bang,” *Nature*, vol. 616, no. 7956, pp. 266–269, 2023. arXiv:2207.12446.
- [31] L. Heisenberg, H. Villarrubia-Rojo, and J. Zosso, “Can late-time extensions solve the H_0 and σ_8 tensions?,” *Phys. Rev. D*, vol. 106, no. 4, p. 043503, 2022. arXiv:2202.01202.
- [32] V. Marra and L. Perivolaropoulos, “Rapid transition of G_{eff} at $z_t \simeq 0.01$ as a possible solution of the Hubble and growth tensions,” *Phys. Rev. D*, vol. 104, no. 2, p. L021303, 2021. arXiv:2102.06012.
- [33] G. Alestas, L. Kazantzidis, and L. Perivolaropoulos, “ $w - M$ phantom transition at $z_t < 0.1$ as a resolution of the Hubble tension,” *Phys. Rev. D*, vol. 103, no. 8, p. 083517, 2021. arXiv:2012.13932.

- [34] L. Perivolaropoulos and F. Skara, “Hubble tension or a transition of the Cepheid SnIa calibrator parameters?,” *Phys. Rev. D*, vol. 104, no. 12, p. 123511, 2021. arXiv:2109.04406.
- [35] G. Alestas *et al.*, “Late-transition versus smooth $H(z)$ -deformation models for the resolution of the Hubble crisis,” *Phys. Rev. D*, vol. 105, no. 6, p. 063538, 2022. arXiv:2110.04336.
- [36] L. Perivolaropoulos and F. Skara, “A Reanalysis of the Latest SH0ES Data for H_0 : Effects of New Degrees of Freedom on the Hubble Tension,” *Universe*, vol. 8, no. 10, p. 502, 2022. arXiv:2208.11169.
- [37] A. Gómez-Valent, A. Favale, M. Migliaccio, and A. A. Sen, “Late-time phenomenology required to solve the H_0 tension in view of the cosmic ladders and the anisotropic and angular BAO datasets,” *Phys. Rev. D*, vol. 109, no. 2, p. 023525, 2024. arXiv:2309.07795.
- [38] R. Calderón, R. Gannouji, B. L’Huillier, and D. Polarski, “Negative cosmological constant in the dark sector?,” *Phys. Rev. D*, vol. 103, no. 2, p. 023526, 2021. arXiv:2008.10237.
- [39] Ö. Akarsu, S. Kumar, E. Özülker, and J. A. Vazquez, “Relaxing cosmological tensions with a sign switching cosmological constant,” *Phys. Rev. D*, vol. 104, no. 12, p. 123512, 2021. arXiv:2108.09239.
- [40] Ö. Akarsu *et al.*, “ Λ_s CDM model: A promising scenario for alleviation of cosmological tensions,” arXiv:2307.10899. arXiv:2307.10899.
- [41] Ö. Akarsu, J. D. Barrow, L. A. Escamilla, and J. A. Vazquez, “Graduated dark energy: Observational hints of a spontaneous sign switch in the cosmological constant,” *Phys. Rev. D*, vol. 101, no. 6, p. 063528, 2020. arXiv:1912.08751.
- [42] J. Grande, J. Solà, and H. Stefancic, “LXCDM: A Cosmon model solution to the cosmological coincidence problem?,” *JCAP*, vol. 08, p. 011, 2006. gr-qc/0604057.
- [43] J. Grande, J. Solà, and H. Stefancic, “Composite dark energy: Cosmon models with running cosmological term and gravitational coupling,” *Phys. Lett. B*, vol. 645, pp. 236–244, 2007. gr-qc/0609083.
- [44] J. Grande, A. Pelinson, and J. Solà, “Dark energy perturbations and cosmic coincidence,” *Phys. Rev. D*, vol. 79, p. 043006, 2009. arXiv:0809.3462.
- [45] C. Moreno-Pulido and J. Solà, “Running vacuum in quantum field theory in curved space-time: renormalizing ρ_{vac} without $\sim m^4$ terms,” *Eur. Phys. J. C*, vol. 80, no. 8, p. 692, 2020. arXiv:2005.03164.
- [46] C. Moreno-Pulido and J. Solà Peracaula, “Renormalizing the vacuum energy in cosmological spacetime: implications for the cosmological constant problem,” *Eur. Phys. J. C*, vol. 82, no. 6, p. 551, 2022. arXiv:2201.05827.
- [47] C. Moreno-Pulido and J. Solà Peracaula, “Equation of state of the running vacuum,” *Eur. Phys. J. C*, vol. 82, no. 12, p. 1137, 2022. arXiv:2207.07111.
- [48] C. Moreno-Pulido, J. Solà Peracaula, and S. Cheraghchi, “Running vacuum in QFT in FLRW spacetime: the dynamics of $\rho_{vac}(H)$ from the quantized matter fields,” *Eur. Phys. J. C*, vol. 83, no. 7, p. 637, 2023. arXiv:2301.05205.
- [49] J. Solà Peracaula, A. Gómez-Valent, J. de Cruz Pérez, and C. Moreno-Pulido, “Running vacuum against the H_0 and σ_8 tensions,” *EPL*, vol. 134, no. 1, p. 19001, 2021. arXiv:2102.12758.

- [50] J. Solà Peracaula, A. Gómez-Valent, J. de Cruz Pérez, and C. Moreno-Pulido, “Running Vacuum in the Universe: Phenomenological Status in Light of the Latest Observations, and Its Impact on the σ_8 and H_0 Tensions,” *Universe*, vol. 9, no. 6, p. 262, 2023. arXiv:2304.11157.
- [51] A. Gómez-Valent, N. E. Mavromatos, and J. Solà Peracaula, “Stringy Running Vacuum Model and current Tensions in Cosmology,” *Class. Quant. Grav.*, vol. 41, no. 1, p. 015026, 2023, arXiv:2305.15774.
- [52] A. Gómez-Valent and J. Solà Peracaula, “ Λ CDM and the cosmological tensions,” in preparation.
- [53] S. Basilakos, N. E. Mavromatos, and J. Solà Peracaula, “Do we Come from a Quantum Anomaly?,” *Int. J. Mod. Phys. D*, vol. 28, no. 14, p. 1944002, 2019. arXiv:1905.04685.
- [54] S. Basilakos, N. E. Mavromatos, and J. Solà Peracaula, “Gravitational and Chiral Anomalies in the Running Vacuum Universe and Matter-Antimatter Asymmetry,” *Phys. Rev.*, vol. D101, no. 4, p. 045001, 2020. arXiv:1907.04890.
- [55] S. Basilakos, N. E. Mavromatos, and J. Solà Peracaula, “Quantum Anomalies in String-Inspired Running Vacuum Universe: Inflation and Axion Dark Matter,” *Phys. Lett.*, vol. B803, p. 135342, 2020. arXiv:2001.03465.
- [56] N. E. Mavromatos, “Geometrical origins of the universe dark sector: string-inspired torsion and anomalies as seeds for inflation and dark matter,” *Phil. Trans. A. Math. Phys. Eng. Sci.*, vol. 380, no. 2222, p. 20210188, 2022. arXiv:2108.02152.
- [57] P. Dorlis, N. E. Mavromatos, and S.-N. Vlachos, “Condensate-Induced Inflation from Primordial Gravitational Waves in String-Inspired Chern-Simons Gravity,” 3 2024. arXiv:2403.09005.
- [58] N. E. Mavromatos, P. Dorlis, and S.-N. Vlachos, “Torsion-induced axions in string theory, quantum gravity and the cosmological tensions,” in *Workshop on the Standard Model and Beyond*, 4 2024. arXiv:2404.18741.
- [59] D. Brout *et al.*, “The Pantheon+ Analysis: Cosmological Constraints,” *Astrophys. J.*, vol. 938, no. 2, p. 110, 2022. arXiv:2202.04077.
- [60] A. G. Riess *et al.*, “A Comprehensive Measurement of the Local Value of the Hubble Constant with 1 km/s/Mpc Uncertainty from the Hubble Space Telescope and the SH0ES Team,” *Astrophys. J. Lett.*, vol. 934, no. 1, p. L7, 2022. arXiv:2112.04510.
- [61] R. Jiménez, L. Verde, T. Treu, and D. Stern, “Constraints on the equation of state of dark energy and the Hubble constant from stellar ages and the CMB,” *Astrophys. J.*, vol. 593, pp. 622–629, 2003. astro-ph/0302560.
- [62] J. Simon, L. Verde, and R. Jiménez, “Constraints on the redshift dependence of the dark energy potential,” *Phys. Rev.*, vol. D71, p. 123001, 2005. astro-ph/0412269.
- [63] D. Stern *et al.*, “Cosmic Chronometers: Constraining the Equation of State of Dark Energy. I: $H(z)$ Measurements,” *JCAP*, vol. 1002, p. 008, 2010. arXiv:0907.3149.
- [64] C. Zhang *et al.*, “Four new observational $H(z)$ data from luminous red galaxies in the Sloan Digital Sky Survey data release seven,” *Res. Astron. Astrophys.*, vol. 14, no. 10, pp. 1221–1233, 2014. arXiv:1207.4541.

- [65] M. Moresco *et al.*, “Improved constraints on the expansion rate of the Universe up to z 1.1 from the spectroscopic evolution of cosmic chronometers,” *JCAP*, vol. 1208, p. 006, 2012. arXiv:1201.3609.
- [66] M. Moresco, “Raising the bar: new constraints on the Hubble parameter with cosmic chronometers at $z \sim 2$,” *Mon. Not. Roy. Astron. Soc.*, vol. 450, no. 1, pp. L16–L20, 2015. arXiv:1503.01116.
- [67] M. Moresco *et al.*, “A 6% measurement of the Hubble parameter at $z \sim 0.45$: direct evidence of the epoch of cosmic re-acceleration,” *JCAP*, vol. 1605, no. 05, p. 014, 2016. arXiv:1601.01701.
- [68] A. Ratsimbazafy *et al.*, “Age-dating Luminous Red Galaxies observed with the Southern African Large Telescope,” *Mon. Not. Roy. Astron. Soc.*, vol. 467, no. 3, pp. 3239–3254, 2017. arXiv:1702.00418.
- [69] N. Borghi, M. Moresco, and A. Cimatti, “Toward a Better Understanding of Cosmic Chronometers: A New Measurement of $H(z)$ at $z \sim 0.7$,” *Astrophys. J. Lett.*, vol. 928, no. 1, p. L4, 2022. arXiv:2110.04304.
- [70] E. Tomasetti *et al.*, “A new measurement of the expansion history of the Universe at $z = 1.26$ with cosmic chronometers in VANDELS,” *Astron. Astrophys.*, vol. 679, p. A96, 2023. arXiv:2305.16387.
- [71] A. Favale, M. G. Dainotti, A. Gómez-Valent, and M. Migliaccio, “Towards a new model-independent calibration of Gamma-Ray Bursts,” 2 2024. arXiv:2402.13115.
- [72] M. Moresco *et al.*, “Setting the Stage for Cosmic Chronometers. II. Impact of Stellar Population Synthesis Models Systematics and Full Covariance Matrix,” *Astrophys. J.*, vol. 898, no. 1, p. 82, 2020. arXiv:2003.07362.
- [73] G. C. Carvalho *et al.*, “Baryon Acoustic Oscillations from the SDSS DR10 galaxies angular correlation function,” *Phys. Rev. D*, vol. 93, no. 2, p. 023530, 2016. arXiv:1507.08972.
- [74] J. S. Alcaniz *et al.*, “Measuring baryon acoustic oscillations with angular two-point correlation function,” *Fundam. Theor. Phys.*, vol. 187, pp. 11–19, 2017. arXiv:1611.08458.
- [75] G. C. Carvalho *et al.*, “The transverse baryonic acoustic scale from the SDSS DR11 galaxies,” *Astropart. Phys.*, vol. 119, p. 102432, 2020. arXiv:1709.00271.
- [76] E. de Carvalho *et al.*, “Angular Baryon Acoustic Oscillation measure at $z = 2.225$ from the SDSS quasar survey,” *JCAP*, vol. 04, p. 064, 2018. arXiv:1709.00113.
- [77] E. de Carvalho *et al.*, “BAO angular scale at $z_{\text{eff}} = 0.11$ with the SDSS blue galaxies,” *Astron. Astrophys.*, vol. 649, p. A20, 2021. arXiv:2103.14121.
- [78] S. Anselmi *et al.*, “Cosmic distance inference from purely geometric BAO methods: Linear Point standard ruler and Correlation Function Model Fitting,” *Phys. Rev. D*, vol. 99, no. 12, p. 123515, 2019. arXiv:1811.12312.
- [79] L. Guzzo *et al.*, “A test of the nature of cosmic acceleration using galaxy redshift distortions,” *Nature*, vol. 451, pp. 541–545, 2008. arXiv:0802.1944.
- [80] Y.-S. Song and W. J. Percival, “Reconstructing the history of structure formation using Redshift Distortions,” *JCAP*, vol. 0910, p. 004, 2009. arXiv:0807.0810.

- [81] C. Blake *et al.*, “The WiggleZ Dark Energy Survey: the growth rate of cosmic structure since redshift $z=0.9$,” *Mon. Not. Roy. Astron. Soc.*, vol. 415, p. 2876, 2011. arXiv:1104.2948.
- [82] C. Blake *et al.*, “Galaxy And Mass Assembly (GAMA): improved cosmic growth measurements using multiple tracers of large-scale structure,” *Mon. Not. Roy. Astron. Soc.*, vol. 436, p. 3089, 2013. arXiv:1309.5556.
- [83] F. Simpson *et al.*, “Galaxy and mass assembly: Redshift space distortions from the clipped galaxy field,” *Phys. Rev.*, vol. D93, no. 2, p. 023525, 2016. arXiv:1505.03865.
- [84] H. Gil-Marín *et al.*, “The clustering of galaxies in the SDSS-III Baryon Oscillation Spectroscopic Survey: RSD measurement from the power spectrum and bispectrum of the DR12 BOSS galaxies,” *Mon. Not. Roy. Astron. Soc.*, vol. 465, no. 2, pp. 1757–1788, 2017. arXiv:1606.00439.
- [85] J. Hou *et al.*, “The Completed SDSS-IV extended Baryon Oscillation Spectroscopic Survey: BAO and RSD measurements from anisotropic clustering analysis of the Quasar Sample in configuration space between redshift 0.8 and 2.2,” *Mon. Not. Roy. Astron. Soc.*, vol. 500, no. 1, pp. 1201–1221, 2020. arXiv:2007.08998.
- [86] K. Said *et al.*, “Joint analysis of 6dFGS and SDSS peculiar velocities for the growth rate of cosmic structure and tests of gravity,” *Mon. Not. Roy. Astron. Soc.*, vol. 497, no. 1, pp. 1275–1293, 2020. arXiv:2007.04993.
- [87] F. Avila, A. Bernui, E. de Carvalho, and C. P. Novaes, “The growth rate of cosmic structures in the local Universe with the ALFALFA survey,” *Mon. Not. Roy. Astron. Soc.*, vol. 505, no. 3, pp. 3404–3413, 2021. arXiv:2105.10583.
- [88] F. G. Mohammad *et al.*, “The VIMOS Public Extragalactic Redshift Survey (VIPERS): Unbiased clustering estimate with VIPERS slit assignment,” *Astron. Astrophys.*, vol. 619, p. A17, 2018. arXiv:1807.05999.
- [89] T. Okumura *et al.*, “The Subaru FMOS galaxy redshift survey (FastSound). IV. New constraint on gravity theory from redshift space distortions at $z \sim 1.4$,” *Publ. Astron. Soc. Jap.*, vol. 68, no. 3, p. 38, 2016. arXiv:1511.08083.
- [90] J. Lesgourgues, “The Cosmic Linear Anisotropy Solving System (CLASS) I: Overview,” 4 2011. arXiv:1104.2932.
- [91] D. Blas, J. Lesgourgues, and T. Tram, “The Cosmic Linear Anisotropy Solving System (CLASS) II: Approximation schemes,” *JCAP*, vol. 1107, p. 034, 2011. arXiv:1104.2933.
- [92] N. Metropolis *et al.*, “Equation of state calculations by fast computing machines,” *J. Chem. Phys.*, vol. 21, pp. 1087–1092, 1953.
- [93] W. Hastings, “Monte Carlo Sampling Methods Using Markov Chains and Their Applications,” *Biometrika*, vol. 57, pp. 97–109, 1970.
- [94] B. Audren, J. Lesgourgues, K. Benabed, and S. Prunet, “Conservative Constraints on Early Cosmology: an illustration of the Monte Python cosmological parameter inference code,” *JCAP*, vol. 1302, p. 001, 2013. arXiv:1210.7183.
- [95] T. Brinckmann and J. Lesgourgues, “MontePython 3: boosted MCMC sampler and other features,” *Phys. Dark Univ.*, vol. 24, p. 100260, 2019. arXiv:1804.07261.

- [96] A. Lewis, “GetDist: a Python package for analysing Monte Carlo samples,” 2019. arXiv:1910.13970.
- [97] D. J. Spiegelhalter, N. G. Best, B. P. Carlin, and A. van der Linde, “Bayesian measures of model complexity and fit,” *J. Roy. Stat. Soc.*, vol. 64, p. 583, 2002.
- [98] H. Akaike, “A new look at the statistical model identification,” *IEEE Trans. Autom. Control*, vol. 19, pp. 716–723, 1974.
- [99] L. A. Anchordoqui, I. Antoniadis, and D. Lust, “Anti-de Sitter \rightarrow de Sitter transition driven by Casimir forces and mitigating tensions in cosmological parameters,” 12 2023. arXiv:2312.12352.
- [100] Ö. Akarsu *et al.*, “ Λ sCDM cosmology from a type-II minimally modified gravity,” 2 2024. arXiv:2402.07716.
- [101] L. A. Anchordoqui *et al.*, “From infinite to infinitesimal: Using the Universe as a dataset to probe Casimir corrections to the vacuum energy from fields inhabiting the dark dimension,” 4 2024. arXiv:2404.17334.
- [102] T. M. C. Abbott *et al.*, “The Dark Energy Survey: Cosmology Results With ~ 1500 New High-redshift Type Ia Supernovae Using The Full 5-year Dataset,” 1 2024. arXiv:2401.02929.
- [103] D. Rubin *et al.*, “Union Through UNITY: Cosmology with 2,000 SNe Using a Unified Bayesian Framework,” 11 2023. arXiv:2311.12098.
- [104] S. A. Adil, U. Mukhopadhyay, A. A. Sen, and S. Vagnozzi, “Dark energy in light of the early JWST observations: case for a negative cosmological constant?,” *JCAP*, vol. 10, p. 072, 2023. arXiv:2307.12763.
- [105] N. Menci *et al.*, “Negative cosmological constant in the dark energy sector: tests from JWST photometric and spectroscopic observations of high-redshift galaxies,” 1 2024. arXiv:2401.12659.